Human Molecular Genetics, 2018, Vol. 27, No. 18 3206–3217

doi: 10.1093/hmg/ddy221
Advance Access Publication Date: 13 June 2018
Original Article

ORIGINAL ARTICLE

Transcriptomic RNAseq drug screen in cerebrocortical cultures: toward novel neurogenetic disease therapies

Jeremiah Hadwen[1,2], Sarah Schock[1,2], Alan Mears[1,2], Robert Yang[3], Philippe Charron[1,2], Liying Zhang[3], Hualin S. Xi[3] and Alex MacKenzie[1,2,*]

[1]Department of Cellular and Molecular Medicine, University of Ottawa, Ottawa, ON K1H8L1, Canada, [2]Children's Hospital of Eastern Ontario Research Institute, Ottawa, ON K1H8L1, Canada and [3]Computational Sciences Centre of Emphasis, Pfizer, Boston, MA, USA

*To whom correspondence should be addressed at: Children's Hospital of Eastern Ontario Research Institute, Apoptosis Research Center, 401 Smyth Road, Ottawa, ON K1H 8L1, Canada. Tel: +1 6137372772; Fax: +1 6137384833; Email: mackenzie@cheo.on.ca

Abstract

Rare monogenic diseases affect millions worldwide; although over 4500 rare disease genotypes are known, disease-modifying drugs are available for only 5% of them. The sheer number of these conditions combined with their rarity precludes traditional costly drug discovery programs. An economically viable alternative is to repurpose established drugs for rare diseases. Many genetic diseases result from increased or decreased protein activity and identification of clinically approved drugs which moderate this pathogenic dosage holds therapeutic potential. To identify such agents for neurogenetic diseases, we have generated genome-wide transcriptome profiles of mouse primary cerebrocortical cultures grown in the presence of 218 blood–brain barrier (BBB) penetrant clinic-tested drugs. RNAseq and differential expression analyses were used to generate transcriptomic profiles; therapeutically relevant drug–gene interactions related to rare neurogenetic diseases identified in this fashion were further analyzed by quantitative reverse transcriptase-polymerase chain reaction, western blot and immunofluorescence. We have created a transcriptome-wide searchable database for easy access to the gene expression data resulting from the cerebrocortical drug screen (Neuron Screen) and have mined this data to identify a novel link between thyroid hormone and expression of the peripheral neuropathy associated gene *Pmp22*. Our results demonstrate the utility of cerebrocortical cultures for transcriptomic drug screening, and the database we have created will foster further discovery of novel links between over 200 clinic-tested BBB penetrant drugs and genes related to diverse neurologic conditions.

Introduction

Rare diseases caused by single-gene mutations are major contributors to human disability and illness. Although by definition, a rare genetic disease affects fewer than 1 in 2000 people (Europe) or fewer than 200 000 people in the USA (1), such diseases are collectively common and pose a significant medical, societal and economic cost (2,3). A recent Italian study found that rare diseases explain 4.2% of the general population years of life lost compared with 1.2% attributable to infectious diseases and 2.6% to diabetes mellitus(4). In the past 10 years, rare disease gene discovery has increased significantly, outpacing the development of rare disease therapeutics (5). The relatively slow development rate of rare genetic disease therapies can in part be attributed to lengthy, costly drug development including an increasingly inefficient drug approval process (6). Although economic incentives from governments and rare

Received: March 17, 2018. **Revised:** May 23, 2018. **Accepted:** June 4, 2018

disease patient groups have prompted an increased interest in developing rare disease therapeutics (7), the gap continues to grow. Furthermore, even when developed, most rare disease drugs are prohibitively expensive (8,9). An alternative to traditional rare disease drug development is to, at roughly one tenth the cost and at least twice the speed (10), repurpose one of the growing number of clinically approved drugs (11).

When rare diseases are viewed as disorders of gene/protein dosage, one credible strategy for drug repurposing focuses on the off-target impact of pharmaceuticals on disease modifying transcript (and thus protein) levels (12,13). This could be the upregulation of mutated recessive disease genes encoding proteins with residual enzymatic activity (and appropriate subcellular localization), of paralogous genes that are sequentially alike, and that functionally recapitulate mutated recessive disease genes, or of genes that cause disease when haploinsufficient. Conversely, the downregulation of mutated dominant genes which confer a gain of pathologic function or of genes that cause disease when present in increased number, may have clinical utility (14). Therefore, clinic-tested drugs that modulate disease gene/protein levels may be effective in treating rare genetic diseases. We recently published a comparison of three methods of screening for promising clinic-ready drug-rare disease gene interactions, establishing their relative yields and validation rates (i.e. whether *in vitro* modulation of transcripts correlated with protein levels). The two computational and one fibroblast-based screens analyzed ∼26 000 and ∼23 000 interactions, respectively, and resulted in the identification of a number of interactions which validated *in vitro* (13).

To identify drug–gene interactions that may be useful for treating rare neurogenetic diseases, we conducted RNA sequencing (RNAseq)-based transcriptome profiling of mouse primary cerebrocortical cultures treated with 218 blood–brain barrier (BBB) penetrant clinic-ready drugs. The resulting dataset was then queried for upregulation of transcripts encoded by neurogenetic disease genes. Positive drug–gene interactions were assessed by quantitative reverse transcriptase-polymerase chain reaction (qRT-PCR) to verify mRNA induction *in vitro* and further investigated in wild-type mice and rats was performed. These investigations have identified a link between thyroid hormone (TH) and upregulation of the peripheral myelin protein 22 (*Pmp22*) (15), haploinsufficiency of which causes the rare hereditary neuropathy with liability to pressure palsies (HNPP). We have also developed an open-access application (the Neuron Screen database) permitting the search of our drug screen differential expression (DE) dataset to assist those studying neurogenetic and other neurologic diseases to identify similar drug–neurogenetic disease gene interactions.

Results

Mouse cerebrocortical culture model

To generate mammalian central nervous system transcriptomic profiles elicited by clinic-ready drugs (16,17), cortices of filial 1 offspring of an FVBN × C3B6F1 cross at embryonic day 16.5 (E16.5) were pooled, triturated and cultured in monolayer. This triple hybrid (3H) mouse strain was created from three phylogenetically dissimilar strains (Jackson Labs) (18) to minimize the transcriptional bias of inbred mice (19) and model the comparatively more diverse genetics of most human populations (16). To evaluate the cell type composition and neuronal synaptic maturity of these 3H cultures, immunofluorescence (IF) staining and electrophysiologic recordings were undertaken at day *in vitro* 21 (DIV21) (20,21). Staining of the 3H cultures for neuron-specific MAP2 and astrocyte-specific ALDH1L1 showed roughly equal numbers of neurons and astrocytes (Fig. 1A) consistent with recent estimates of human cortex glial-to-neuron ratio (GNR) (22) and rat cortical cultures (20). The 3H cultures also contained a variety of GABAergic interneurons as evidenced by staining for neuronal nitric oxide synthase (nNOS), parvalbumin and calretinin (Fig. 1B). Staining for the microglia marker IBA1 and the endothelial marker VE-cadherin was negative. Cortical neuron synaptic maturity was confirmed by the punctate staining pattern of synaptic markers vesicular glutamate transporter (vGLUT) and vesicular GABA transporter (vGAT) (Fig. 1C). Microelectrode array (MEA) recordings of 3H cultures at three stages of maturation demonstrated an increased frequency and synchrony of synaptic depolarizations at DIV21 also reflecting relative electrophysiologic maturity (Fig. 1D). The three GABAergic interneuron subtypes detected by IF analysis (23,24), the mature cortical synapses reflected by vGAT and vGLUT punctate staining (20), and the highly synchronous firing on MEAs characteristic of full cortical network maturity (25) all support the physiologic relevance of the 3H cortical culture system.

RNAseq drug screen

For the Neuron Screen, two hundred and seven drugs were selected from the Screen-Well FDA approved drug library v2 (Enzo Life Sciences) using three criteria: published reports of BBB penetrance, comparative safety consistent with long-term use and oral bioavailability. Another 11 Pfizer shelved phase II compounds were also included in the screen and 9 vehicle controls as well. The drugs used in the screen represent 80 therapeutic classes (Supplementary Material, Fig. S1).

After individual treatment of 3H cultures for 8 h (drug or vehicle), complementary DNA (cDNA) libraries, constructed from the poly-A fraction of total RNA extracted from drug and control treated 3H cultures, were sequenced, analyzed and organized to establish a transcriptome-wide DE dataset representing all 227 sequenced libraries. For each sample, gene expression for ∼14 000 genes with cpm >1 was normalized against the average of all conditions. Given that the screen was performed as a single replicate, the expression of a given gene across all samples served as the background to represent unaffected expression distributions. Robust *z*-scores and adjusted *P*-values (*P*-adj) for each potential drug–gene interaction were generated, with DE being defined as *P*-adj <0.05.

Quality control analysis revealed that more than 99% of the transcripts in the dataset were poly-adenylated (Supplementary Material, Table S1). An average of 114 genes were modulated in the drug treatment group compared with 12 in the control treatment group (Fig. 2A); in contrast the median number of responsive genes was roughly equal (21 and 22, respectively) indicating that most of the drugs modulated a small proportion of the neuronal transcriptome. The twenty-one (10%) strongest perturbagens and associated number of differentially expressed genes (DEGs) are shown in Figure 2B; the top 5 drugs (fenofibrate, nilotinib, ciprofibrate, aminophylline and diflunisal) modulating >1000 genes each. Principal component analysis (PCA) of gene expression for the 227 libraries revealed no shared principal components underlying a large portion of the gene expression variance for most drugs assayed (Supplementary Material, Fig. S2), suggesting a diverse set of transcriptomic responses. However, the libraries for several of the top perturbagens (i.e. fenofibrate, nilotinib, diflunisal, ciprofibrate) diverge from the other drug and vehicle-treated libraries. Furthermore, DAVID

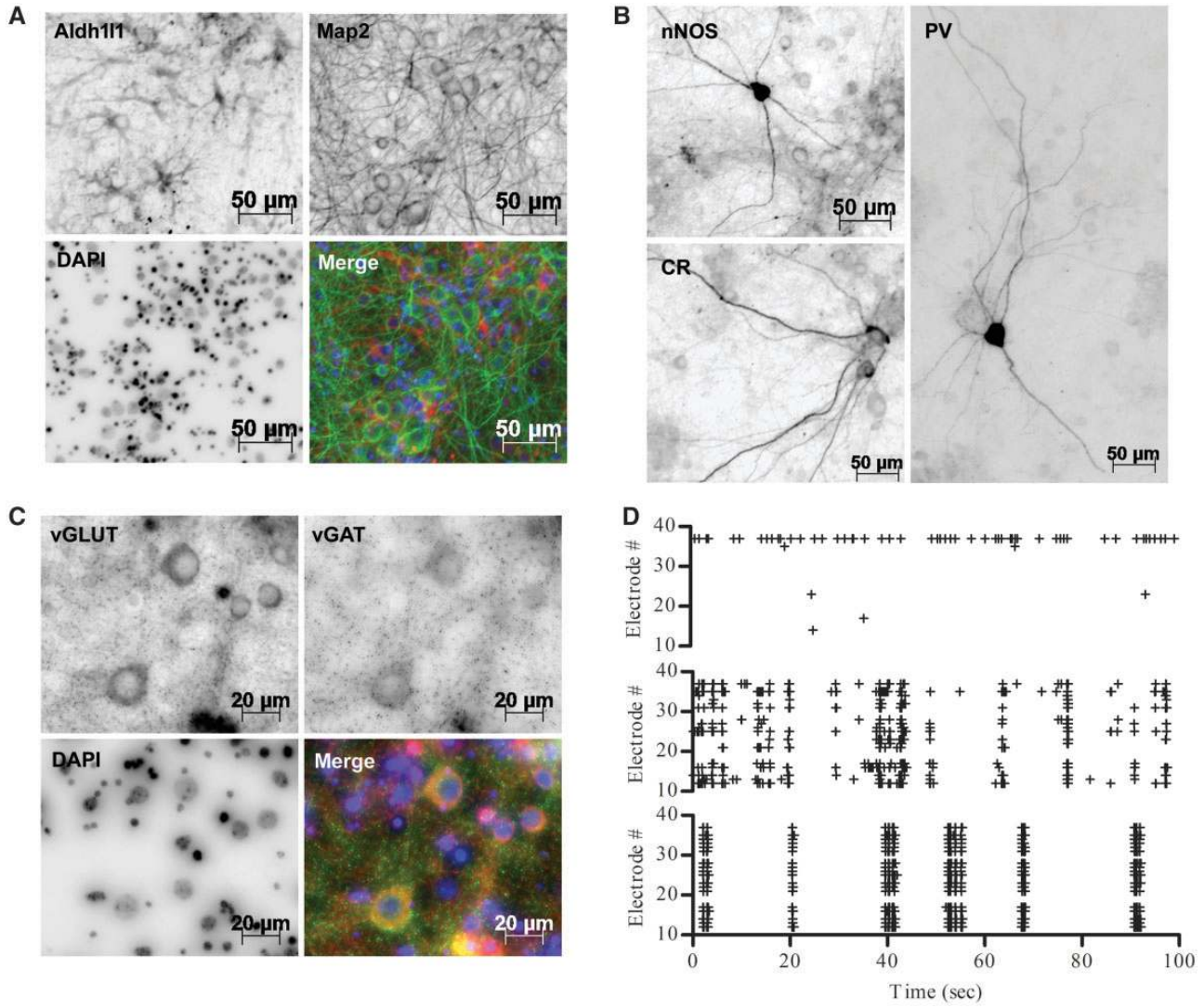

Figure 1. Immunologic and electrophysiologic characterization of the DIV21 3H cortical culture system. **(A)** ×10 magnification of cortical cultures shows neurons (MAP2, green), astrocytes (Aldh1L1, red) and nuclei (DAPI, blue). **(B)** Cortical cultures stained for nNOS, calretinin (CR) or parvalbumin (PV). **(C)** ×20 magnification of cortical cultures shows punctate vGLUT (red), vGAT (green), and nuclear DAPI (blue) staining. **(D)** Raster plots of electrical recordings on a glass microelectrode array are shown at DIV7 (upper), DIV15 (middle) and DIV21 (lower panel). Each cross represents burst activity for the corresponding electrode and time-point.

Functional Annotation Tool was used to conduct enrichment analysis of biologic processes or cellular components (CC) for DEGs from the top five drugs (26,27); 'endoplasmic reticulum (ER) stress', 'apoptosis signaling in response to ER stress', and 'cell cycle arrest' were overrepresented for the upregulated genes while the downregulated genes were enriched for 'CC of post-synaptic membranes' and 'ion transport'.

Validation of RNAseq data

Bioinformatic analyses and cellular toxicity studies were next used to explore the reliability of the Neuron Screen DE data. The upstream regulator analysis (URA) function of ingenuity pathway analysis (IPA) (28) was used to identify agents most likely to elicit the transcriptome signatures of four Neuron Screen agents from two well-characterized drug classes; thyroid analogs [liothyronine (T3) and levothyroxine (T4)] and corticosteroids [DEX and betamethasone (BMZ)]. This revealed both significant within class overlap as well as identifying L-triiodothyronine (structurally identical to T3) and three different steroids (DEX, corticosterone and fluticasone) as the upstream regulators of the thyroid analog and corticosteroid class profiles, respectively (Fig. 3), attesting to the validity of our dataset.

Dose dependent toxicity of four of the top transcriptionally active molecules was next assessed using the lactate dehydrogenase (LDH) assay. At the doses used for the Neuron Screen, only fenofibrate (the top transcriptional modulator in the screen) led to a statistically significant increase in cell death after 14-h treatment (Supplementary Material, Fig. S4). Despite this observation, for reasons outlined in the discussion, we believe the fenofibrate elicited transcriptome may have some utility; nonetheless, the drug–gene hits identified with this compound were not further explored.

Investigation of neuron screen drug–gene hits

To identify transcript-modulating repurposing candidates for rare neurogenetic diseases, we sought drugs that upregulate

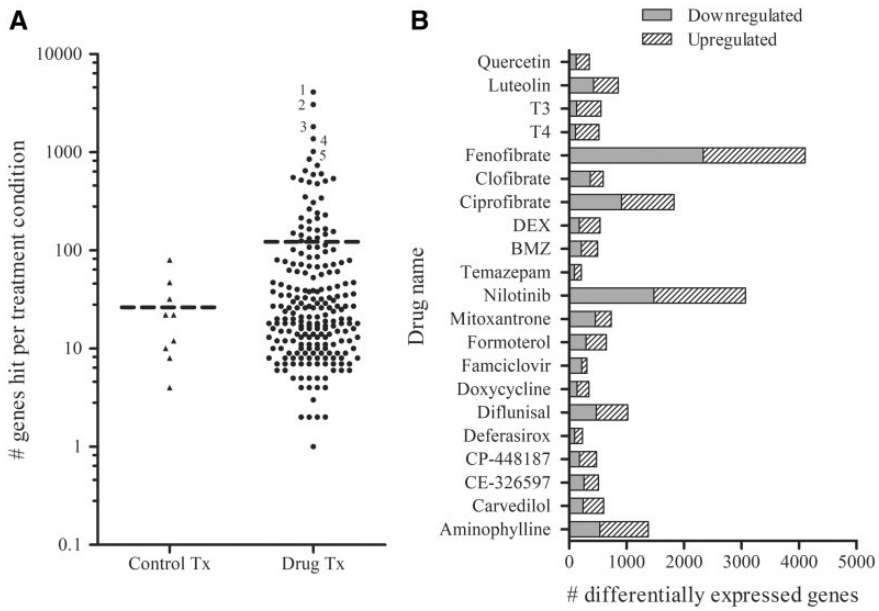

Figure 2. Quantification of drug mediated transcriptome perturbation in 3H cortical cultures. (**A**) The number of statistically significant transcript perturbations (*P*-adj <0.05) for each drug. Each triangle represents a control-treated library, each circle represents a drug-treated library. Hashed lines are the mean number of genes expressed for the control- and drug-treated groups. The top five transcriptionally active drugs are numbered: 1, fenofibrate; 2, nilotinib; 3, ciprofibrate; 4, aminophylline; 5, diflunisal. (**B**) Histogram representing gene perturbations for the 21 drugs with the greatest impact on the neuronal transcriptome.

($P < 0.05$, z-score >3) 60 of the clinically tractable rare disease genes catalogued by Mears *et al.* (13). In addition to being potential targets for pharmacologic gene therapy [as outlined by Mears *et al.* (13)], these 60 genes are linked to rare diseases with a neurologic phenotype that could benefit from gene upregulation, and most have no curative treatment or active clinical trials (Supplementary Material, Table S2). Thirty-two drug–gene interactions were identified in this fashion (Fig. 4A); these treatments were repeated in 3H cortical cultures under the screen conditions followed by qRT-PCR measurement of the specific mRNA. Six of the 32 interactions, ∼20%, validated ($P < 0.05$); half of these [nilotinib (10 μM)-*Sacs*, aminophylline (90 μM)-*Aldh18a1* and T4 (0.2 μM)-*Pmp22*] conferred a ∼2-fold average upregulation of transcript (Fig. 4B–F).

The TH-Pmp22 interaction was further assessed *in vitro* and *in vivo*; given PMP22 protein is primarily expressed in myelinating Schwann cells, primary rat dorsal root ganglion (DRG) cultures were treated with T3 analog of TH (and not T4, as Deiodinase II that converts T4 to the more active T3 is not consistently expressed in the peripheral nervous system) (29,30). IF staining of DIV28 DRG cultures showed highly intertwined neurons (β-III tubulin positive) indicative of a mature DRG culture (Supplementary Material, Fig. S5). Cultures were treated for three weeks with T3 (10, 31.6, 100 nM); qRT-PCR analysis showed ∼50% increase in *Pmp22* mRNA for all treatments (Fig. 5A). Although IF staining of PMP22 was too faint to detect expression in myelin, the presence of cells with perinuclear staining pattern of PMP22 typical of non-myelinating Schwann cells was observed (31) (Fig. 5C–F). Signal intensity of PMP22 could not be rigorously quantitated owing to high background signal, but quantification of total PMP22-stained cells showed a trend toward upregulation for all three T3 doses (Fig. 5B).

The drug–gene pairings that transcriptionally validated in cell culture (nilotinib-*Sacs*, aminophylline-*Aldh18a1*, DEX-*Hsd17b4*, TH-*Pmp22* and diflunisal-*Slc6a8*) were next tested in wild-type mice (C57BL6) or rats (Sprague-Dawley) with intraperitoneal injections or oral gavage doses equivalent to the highest tolerated in humans (Supplementary Material, Methods). qRT-PCR-based measurement of cortical transcript for the five drug–gene pairings studied, identified an increase for the TH-*Pmp22* pairing; Sprague-Dawley rats dosed with 300 μg T4 showed a ∼25% upregulation of *Pmp22* in cortex (Fig. 6A). Furthermore, three well-characterized TH-responsive genes—i.e. Hairless (*Hr*), Sonic hedgehog (*Shh*) and Semaphorin 7a (*Sema7a*) (32,33) that were upregulated in 3H cultures in response to T4 (RNAseq data), were also upregulated (≥2-fold) in the cortex of T4-treated rats (Fig. 6B).

Drug screen database

Using the R-studio Shiny package, we have created a user-friendly interactive website database to enable researchers to mine the Neuron Screen data from the 218 drug treatment expression profiles (∼3 M drug–gene interactions), for interactions of their choice. The 'Primary mouse cortical culture RNAseq drug screen database' can be searched by drug, gene symbol or Ensembl gene ID, and the z-score cutoff adjusted for output. The database provides the user with the identities of the interacting drugs or genes (depending on their query), the dose of the drugs and the associated z-score and adjusted *P*-value of the drug–gene interactions (Fig. 7). It can be freely accessed at 'bigbear.med.uottawa.ca:1000'.

Discussion

There exists a growing gap between the number of molecularly defined rare diseases and effective therapies for these conditions. One potentially generalizable means of addressing this problem is the pharmacologic modulation of specific disease related genes, redressing the pathogenic dysregulated protein levels (and activity), an approach that has been previously proposed for a number of rare genetic diseases. The observation

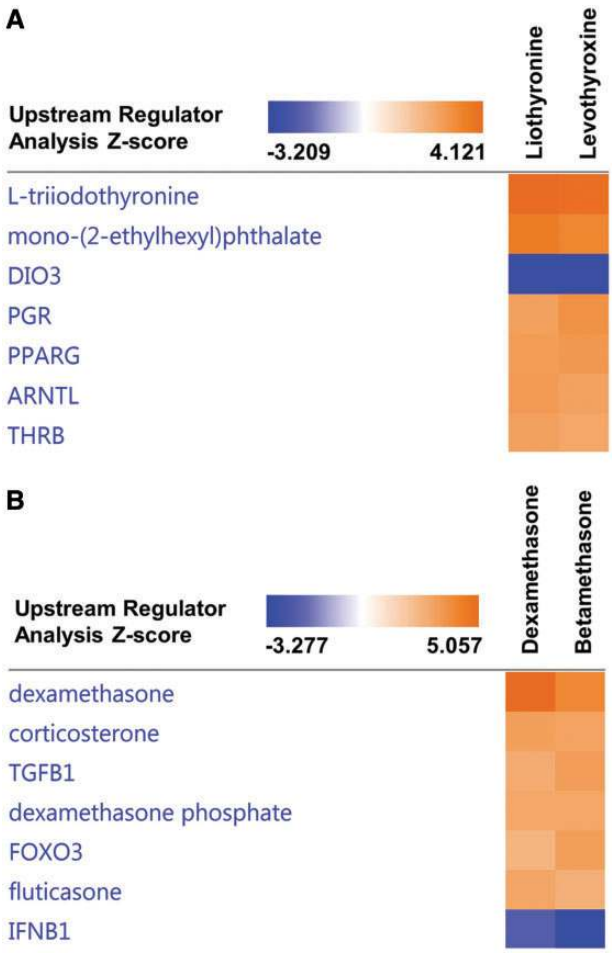

Figure 3. Comparison of neuronal transcriptomic drug-class effects. Transcriptome data for T3, T4, DEX and BMZ treated cultures was assessed using IPA to identify upstream regulators (agents which are the most likely to lead to the observed signature) resulting in the identification of (**A**) L-triiodothyronine (structurally identical to T3) for both the T3 and T4 profiles and (**B**) three different steroid compounds for the DEX and BMZ signatures; DEX itself, corticosterone and the halogenated steroid, fluticasone.

70 years ago of the beneficial effect of persistent fetal gamma hemoglobin on sickle cell disease has led to long standing efforts to induce this hemoglobin beta paralog for diverse hemoglobinopathies (34). The upregulation of paralogs for Duchenne muscular dystrophy (35) and X-linked adrenoleukodystrophy (36) have also been proposed while induction of SMN2 for spinal muscular atrophy has become a clinical reality (37). Pharmacologic gene induction has also been suggested for haploinsufficient disorders; estrogen treatment of the epistaxis associated with hereditary hemorrhagic telangiectasia (38) as well as a number of compounds demonstrating induction of GRN to treat frontotemporal dementia (39). To broaden this approach to additional neurogenetic conditions, we have performed system wide RNAseq analysis of a primary mixed neuronal glial cell system cultured in the presence of 218 drugs and then studied specific transcripts encoded by rare disease related genes as a proxy for protein. A 1:1 GNR, three GABAergic interneuron subtypes and the highly synchronous firing on MEAs characteristic of full cortical network maturity (25) all support the physiologic relevance of the 3H cortical culture system.

Our study of 218 drug-induced neuronal transcriptomes revealed that 5 agents collectively account for almost half of the DE genes (in descending order: fenofibrate, nilotinib, ciprofibrate, aminophylline and diflunisal). PCA revealed that four of these drugs induced gene expression patterns that deviated noticeably from the primary gene expression cluster. Furthermore, bioinformatic analysis (using DAVID) of genes upregulated by all 5 drugs revealed 21% enrichment in genes associated with ER stress (40–42), intrinsic apoptosis signaling, and cell cycle arrest while similar analysis of downregulated genes revealed over 50% are involved in post synaptic membrane and ion transport functions. However, only fenofibrate (80 μM) led to overt cytotoxicity in cortical neurons. Similarly, the top five perturbagens had only 57 responsive genes (42 upregulated and 15 downregulated) in common suggesting that simple cell stress was not the reason for most of the observed DE. In keeping with this, a recent study has documented altered expression of ∼4000 transcripts, close to the number of DE genes in our study, in prefrontal cortex of fenofibrate-treated mice (43). Furthermore, other reports both in neuronal and non-neuronal cells have also shown broad transcriptomic impact of these drugs with no reported cytotoxicity (43–45). Interestingly, as potent neuronal perturbagens as these agents are, they rank no higher than 71st percentile (nilotinib) and as low as 17th percentile (ciprofibrate) in the connectivity map ranking of perturbagens employing a number of immortalized cell lines (46). Thus, ER stress gene activation in the Neuron Screen may highlight the difference in sensitivity that exists between primary neuron cells and immortalized cancer cells.

One method of transcriptomic DE gene data validation in an experimental system is identifying an anticipated (e.g. HDAC inhibitor) expression signature as a positive control (47). In this regard, highly similar transcriptional effects of both two TH analogs and two corticosteroids as well as aligning with the published transcriptomic impact of both drug classes was observed, attesting to the validity of our screen. Furthermore, the validation of ∼20% mRNA inducing drug gene interactions (Supplementary Material, Fig. S4) is double that recently documented for a similar fibroblast screen and four times that identified from connectivity map data (13). Although the 32 hits were identified with a *P*-adj <0.05, only those with *P*-adj <0.01 validated at the transcript level; moreover, for hits with a *P*-adj <0.01, the validation rate increased by 50% with no decrease in statistical power suggesting that the more stringent statistical cutoff might be optimal when analyzing the Neuron Screen data.

The effect of TH on *Pmp22* gene expression is a novel finding and one that requires further investigation. Of the five hits that validated in 3H cortical cultures, T4-*Pmp22* drug–gene combination was the most promising, leading to a statistically significant and potentially therapeutically relevant 25% upregulation in whole animal studies (14). This was accompanied by a >2-fold upregulation of three TH-responsive genes, reflecting supra-physiologic cortical levels of TH in treated rats (48). Given HNPP chiefly impacts the PNS, we next assessed the effect of TH in rat PNS cultures; T3 (100 nM) led to a ∼50% upregulation of Pmp22 transcript and an increase in PMP22 stained cells. Interestingly, there appears to be a plateau effect of TH on *Pmp22* as similar gene expression was observed across the T3 dose–curve, potentially representing saturation of the gene's TH receptor binding elements (49).

Although TH has not been previously related to PMP22 expression, a recent case report detailed HNPP symptoms worsening with a diagnosis of hypothyroidism and markedly improved with TH treatment (50). Exploration of the impact of TH on haploinsufficient *Pmp22* mice with HNPP-like disruption of

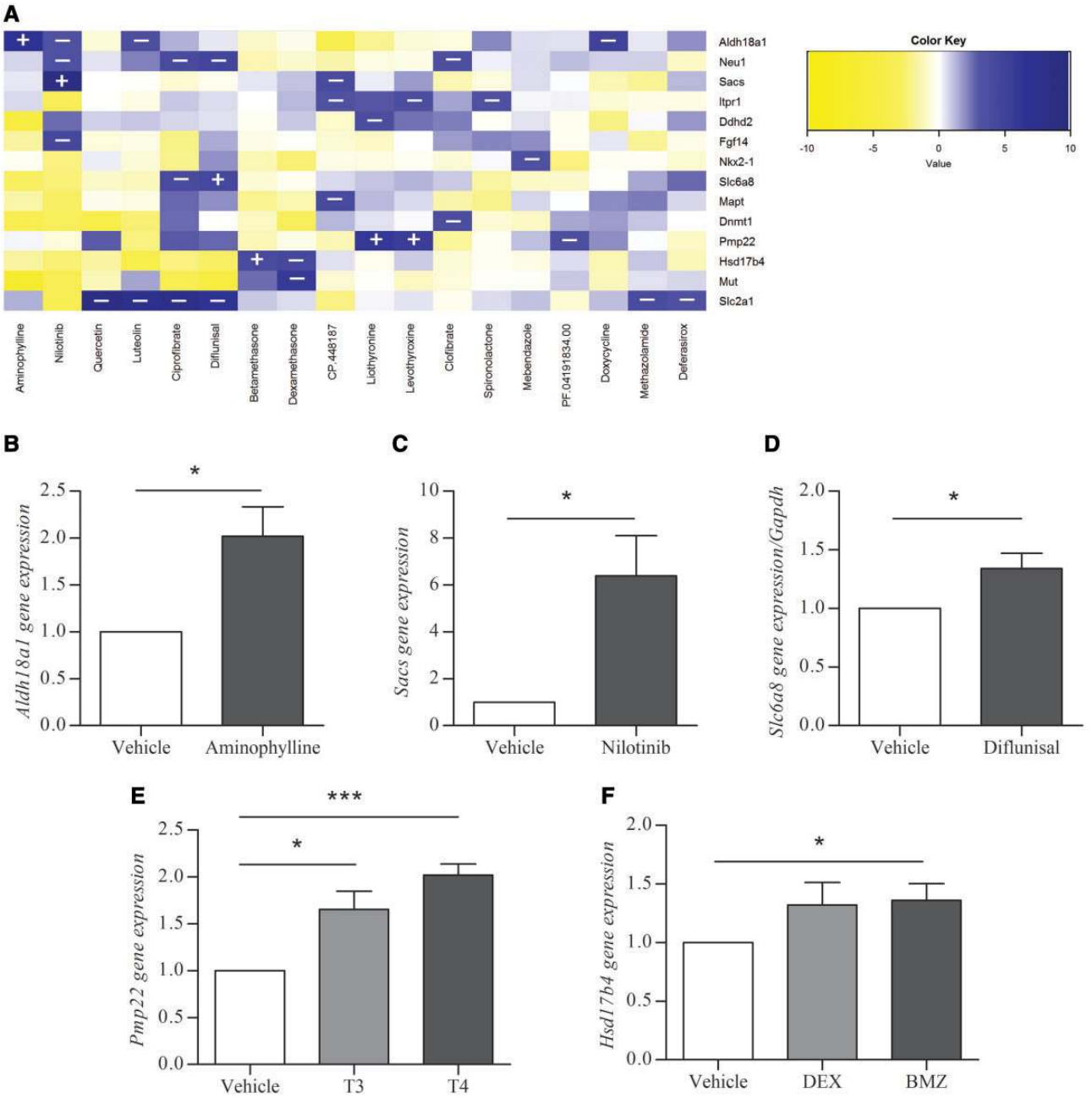

Figure 4. Investigation of 32 neurogenetic drug–gene hits by qRT-PCR in 3H cultures at DIV21 after 8-h treatment. (**A**) Heatmap representing the 32 neurogenetic drug–gene hits where (+) signs indicate drug–gene hits that were validated ($n > 5$, $P < 0.05$) and (−) signs indicate hits that were not upregulated ($n > 2$, $P > 0.05$). (**B**) 90 μM aminophylline upregulates *Aldh18a1* ($n = 7$); (**C**) 10 μM nilotinib upregulates *Sacs* ($n = 8$); (**D**) 200 μM diflunisal upregulates *Slc6a8* ($n = 7$); (**E**) 0.01 μM T3 ($n = 5$) and 0.2 μM T4 ($n = 7$) upregulate *Pmp22*; (**F**) 0.5 μM DEX ($n = 6$) and 0.4 μM BMZ ($n = 7$) upregulate *Hsd17b4*. Target gene expression was normalized against *Gapdh* and shown as treated over vehicle (0.2% DMSO) expression. Statistical analysis was performed by student's two-tailed unpaired t-test $^*P < 0.05$, $^{***}P < 0.001$.

PNS myelination (51) may be of value; ultimately HNPP clinical trials employing thyromimetic compounds (thus avoiding iatrogenic hyperthyroidism) as has been proposed for the treatment of X-ALD (36,52) may be an option. Conversely clinicians may want to proceed cautiously when considering thyroid therapy for patients with Charcot–Marie–Tooth disease type 1A, a condition caused by *PMP22* gene duplication and resulting pathogenic overexpression of the protein (15).

In conclusion, the demonstration of T4 mediated Pmp22 upregulation in rat cortex serves as a validation of our primary cerebrocortical culture and screen as a means of identifying clinically relevant drug–gene interactions as a prelude to the potential repurposing of drugs for rare neurogenetic diseases. In addition to modulation of individual rare disease-associated transcripts, transcriptomal profiles can also serve as therapeutic targets (53,54). Whether through identifying drugs that either impact individual genes or generate neuronal transcriptomes that are orthogonal to disease transcriptional profiles (55), the Neuron Screen database will enable the identification of novel therapeutic leads for rare neurogenetic diseases as well as serve as a valuable resource for the broader neuroscience community.

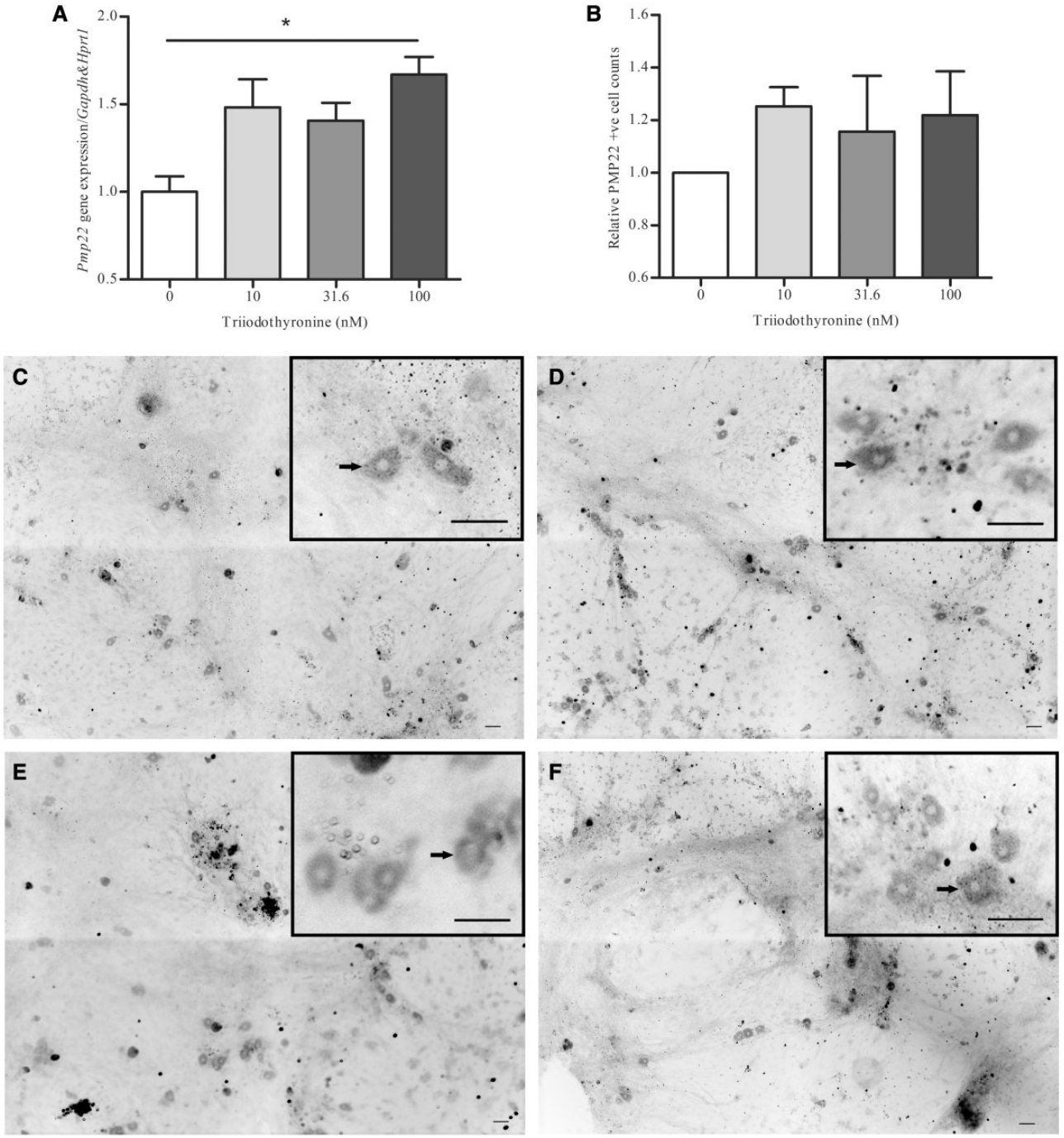

Figure 5. Effect of T3 on Pmp22 transcript and protein levels in DRG cultures. Rat DRG cultures were grown *in vitro* for 7 days and then for an additional 21 days in the presence of vehicle (0.1% DMSO) or half-log dose–curve of T3 (10, 31.6, 100 nM). (**A**) qRT-PCR showing the effect of 21-day treatment of T3 on *Pmp22* transcript levels ($n = 3$). (**B**) Whole-well blinded cell counts (96-well format) of IF stained Pmp22-containing cells normalized to DAPI signal intensity. Cell counts, and counterstain signal intensity quantified by ImageJ ($n = 3$). (**C**) Representative images of DRG cultures [quantified in (B)] with inset magnified images and arrows indicating representative Pmp22-stained cells treated with 0.1% DMSO, (**D**) 10 nM T3, (**E**) 31.6 nM T3, (**F**) 100 nM T3. Images acquired on EVOS FL Auto 2, scale bars represent 50 μm. Error bars indicate SEM and statistical significance was measured by one-way ANOVA (non-parametric) with Tukey post hoc analysis (*$P < 0.05$).

Materials and Methods

Animal care and treatments

All protocols were approved by the Animal Care and Veterinary Services (ACVS) and Ethics board of the University of Ottawa. The female FVB/N and male C3B6F1 mice used for generating embryos for cerebrocortical cultures were supplied by Jackson Labs. Animals were housed in triplicate and given food and water *ad libitum*. For *in vivo* drug studies, male C57BL6 mice (8 weeks old) and male Sprague-Dawley rats (8 weeks old) were obtained from Charles River. Mice and rats were treated daily as per the details found in Supplementary Material, Note S1. T4 treatments were performed in rats whereas mice were used for the other four drugs [aminophylline, dexamethasone (DEX),

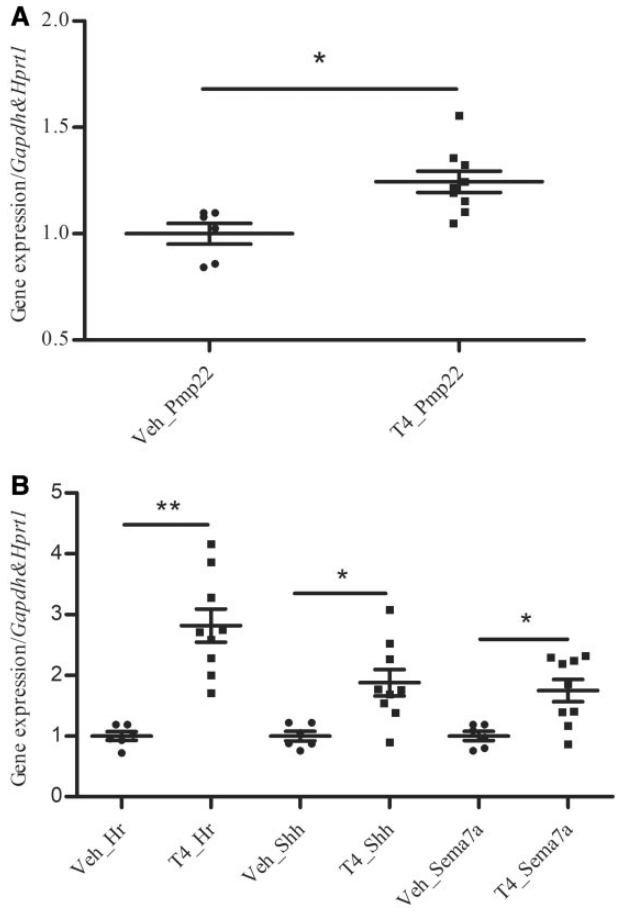

Figure 6. Effect of T4 on *Pmp22* expression in cortex of T4-treated rats. Adult male Sprague-Dawley rats were treated with daily T4 i.p. injections (300 μg/kg) for 8 days. Cortical tissue was subsequently harvested, and total RNA extracted for qRT-PCR assessment of (**A**) *Pmp22* and (**B**) *Hr*, *Shh* and *Sema7a*. Target gene expression, normalized to house-keeping genes (*Gapdh* and *Hprt1*) ±SEM is shown ($n = 6$–9, $^*P < 0.05$). Statistical analysis was performed by student's two-tailed unpaired *t*-test.

diflunisal, nilotinib]. At the end of each treatment experiment, ~4 h after the last dose, animals were anesthetized by isoflurane and euthanized by cervical dislocation (mice) or decapitation (rats). Cortex was collected from each animal and flash-frozen in liquid nitrogen. RNA was extracted by Qiazol lysis reagent and purified through RNeasy Mini spin columns. Gene expression of the corresponding gene (based on *in vitro* drug–gene hit validation, Fig. 4), was evaluated by qRT-PCR (Supplementary Material, Note S6).

Tissue culture

Mouse 3H cortical cultures

Female FVB/N mice were crossed with male C3B6F1 to create 3H embryos. Female and male mice were singly housed and given food and water *ad libitum* before and after initiation of timed mating. Precise timed mating was verified by the presence of a vaginal plug (embryonic day 0.5) by experienced animal technicians. Dams were sacrificed at E16.5 by isoflurance and cervical dislocation. Neuronal culture was performed as previously described (20). Briefly, cortex was isolated from E16.5 embryos and cultured for 21 days on 6- and 96-well poly-D-lysine (PDL, 50 μg/ml) coated polystyrene plates and maintained in Neurobasal medium containing B27 supplement (2%), GlutaMAX (2%), 100 IU/ml penicillin and 100 μg/ml streptomycin. Plating densities were 1E6 and 6E4 cells per well for the 6- and 96-well plates, respectively. Further 3H tissue culture details are provided in Supplementary Material, Note S2.

Dorsal root ganglion

Cryopreserved rat DRGs were purchased from QBM Cell Science. DRGs were grown on 12-well (60 000 cells/well) and 96-well (5000 cells/well) plates coated overnight with PDL (50 μg/ml) and subsequently with laminin (20 μg/ml) for 1 h at 37°C. DRG cultures were seeded in Neurobasal medium containing B27 supplement (2%), GlutaMAX (2%), 100 IU/ml penicillin, 100 μg/ml streptomycin and 50 ng/ml nerve growth factor. A 50% media change was performed after 4 days, and subsequent 75% media changes were performed every 2–3 days. After 7 days *in vitro*, media was supplemented with 50 μg/ml ascorbic acid (AA) to induce myelination and treated with DMSO (0.1%) or T3 (10, 31.6, 100 nM) (56). Cultures were maintained for 21 or 28 days *in vitro* after addition of AA and T3 with 75% media changes containing fresh AA +DMSO or AA +T3 every 2–3 days until harvesting.

Immunofluorescence

IF staining was performed on cortical cultures (DIV21) in 96-well polystyrene plates. Cells were fixed in 4% formaldehyde containing 7% (v/v) picric acid for 20 min at room temperature (20). Primary antibody incubation was performed using the vibration technique (57). Details on IF staining and antibodies are provided in Supplementary Material, Note S3.

Neuronal network recordings

Network extracellular electrophysiologic recordings of cortical cultures were performed with an MEA system from MultiChannel Systems. Triple hybrid mouse cortical cultures were grown on PDL (50 μg/ml) and laminin (20 μg/ml) coated glass MEAs and recordings were obtained as described by Schock *et al.* (20). Recordings were taken at DIV7, DIV15 and DIV21 and performed for a total of 300 s on each day from all 60 electrodes on the MEA. Analysis of burst frequency and synchrony was done by using the software SpAnNer [as outlined by Otto *et al.* (58) and Illes *et al.* (59)].

RNAseq neuron drug screen

Drug treatments

For the drug screen, 3H cortical cultures (DIV21) in 6-well plates were treated for 8 h with vehicle (0.2% DMSO) or one of the 218 BBB-penetrant drugs used for the screen. A total of 207 drugs were selected from the Screen-well v2 FDA approved drug library (Enzo Life Sciences) and 11 Pfizer shelf compounds were included in the screen. Drug concentrations approximating those attained in patients and guided by the literature (60) were used and are provided at bigbear.med.uottawa.ca: 1000 as part of the 'Primary mouse cortical culture RNAseq drug screen database'. Details on drug treatments are provided in Supplementary Material, Note S4.

cDNA library preparation and RNA sequencing

Complementary DNA (cDNA) libraries were created using the KAPA Biosystems Stranded mRNAseq kit from high-quality RNA samples (RIN ≥ 8). Details on library preparation and sequencing are provided in Supplementary Material, Note S5.

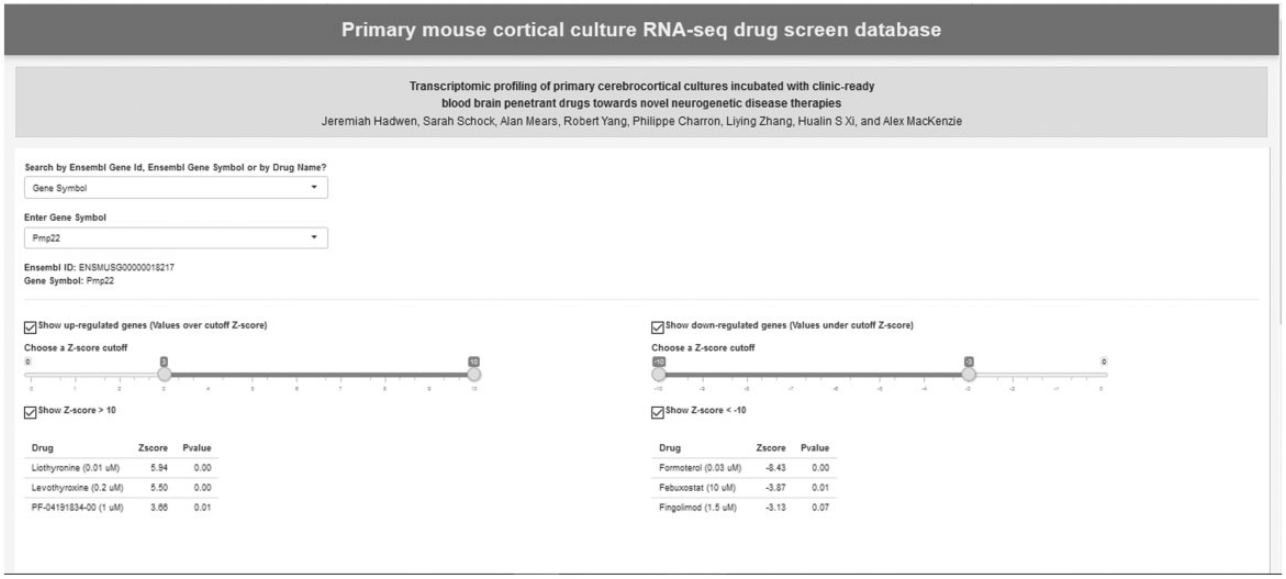

Figure 7. The Neuron Screen database. The database was creating using the Rstudio Shiny app. The transcriptome-wide DE results for each drug treatment from the Neuron Screen were included. The left side has two drop-down menus to facilitate the search of a drug or gene of interest (Ensembl ID or gene symbol). Scale bars allow the user to select the statistical range of their choice (z-score |1| to |10|) for hits. Alternatively, only hits with a z-score>|10| can be seen by clicking the Show z-score-|10|. An example is shown with the gene Pmp22 selected and a cut-off of z-score>|3|.

Bioinformatics

DE analysis

Fastq files from Illumina sequencing were aligned to the mm10 reference genome using Star (version 2.4.0). All fastq files were validated to be single-stranded and reverse-stranded. Read counts were summarized to gene-level by the feature count module of Subread package (version 1.4.6). All samples passed quality control based on post-alignment metrics using RSeQC (version 2.6.1). Genes that had raw counts =0 and/or counts per million (cpm) <1 across all 227 samples were excluded from the final results. Normalization was performed using limma/EdgeR package (version 3.10.5). Briefly, two levels of normalization were performed to adjust for: (i) library size; (ii) mean–variance heteroscedasticity. The trimmed mean of *M*-values method was used to calculate a weighted trimmed mean across all samples (61). Mean–variance relationship was estimated by the Voom module. PCA was calculated to check for systemic bias across samples. The top four principle components were removed, and the resultant residuals were used for subsequent analysis. Robust z-scores were calculated for each gene. P-values were calculated using two-tailed test and multiple-testing adjusted by the Benjamini Hochberg method (62). Drug-induced differential gene expression was defined by an adjusted *P*-value (*P*-adj.) <0.05.

Ingenuity pathway analysis

The transcriptome-wide DE datasets from T4, T3, BMZ and DEX were entered individually into the IPA software (Qiagen Bioinformatics). The two metrics of DE that were entered were 'z-score' and 'P-adj', and data entered were limited to an absolute z-score greater >3. Each dataset was then individually analyzed by IPA using default settings on the analysis tool. After analysis, the IPA comparison tool was used to determine the similarities between the transcriptional perturbations caused by levothyroxine (T4) and T3 and by the perturbations caused by DEX and BMZ. Comparison between drugs in each class was done by using the URA heatmap function.

Quantitative RT-PCR

qRT-PCR was used to investigate the validity of hits from the Neuron Screen in cortical cultures, in DRGs, and in whole mouse and rat experiments. Gene-specific primers were designed for each gene of interest and *Gapdh* & *Hprt1* were used as housekeeping genes. Primers available upon request. Complete qRT-PCR protocol is provided in Supplementary Material, Note S6.

LDH assay

The CytoTox 96 Non-Radioactive Cytotoxicity Assay (Promega) was used to determine the cellular toxicity of five Neuron Screen drugs on the 3H cortical culture system (96-well format cultures). Cultures at DIV21 were treated with half-log doses of fenofibrate, nilotinib, aminophylline, diflunisal for 8 or 14 h. The LDH assay was performed as per the kit specifications. Absorbance at 490 nm was used measure LDH in the culture media, on the SpectraMax 340 Microplate Reader (Molecular Devices). Media from living treated and non-treated cells was normalized to media from cells after complete cell death by freeze–thaw.

Statistical analysis. Statistical analysis of single pair-wise comparisons was calculated by unpaired two-tailed *t*-test with 95% CI, and the null hypothesis was rejected at $P < 0.05$. For multiple pair-wise comparisons performed by qRT-PCR, one-way ANOVA was performed with Tukey post hoc test and 95% CI with null hypothesis rejected at $P < 0.05$. Statistics for DE-RNAseq are summarized in the Differential analysis section.

RNAseq data deposition

The raw sequencing fastq files generated by RNAseq and analyzed to create the Shinny DE database are available from the

Gene Expression Omnibus (GEO) database (accession number GSE110256).

Supplementary Material

Supplementary Material is available at *HMG* online.

Acknowledgements

The authors would like to thank Kate Daniels for her technical help with neuronal dissections and cDNA library preparations, Janice Chin and Lyn Jones for compound selection and advice on the study design, and Steve Baird for assistance with hosting the Shiny database application.

Conflict of Interest Statement: None declared.

Funding

This work was supported by Genome Canada; the Canadian Institutes of Health Research; the Ontario Genomics Institute (OGI-049); Ontario Research Fund; Genome Quebec; Genome British Columbia; and Childrens' Hospital of Eastern Ontario (CHEO) Foundation and performed under the Care4Rare Canada Consortium.

References

1. Beaulieu, C.L., Samuels, M.E., Ekins, S., McMaster, C.R., Edwards, A.M., Krainer, A.R., Hicks, G.G., Frey, B.J., Boycott, K.M. and Mackenzie, A.E. (2012) A generalizable pre-clinical research approach for orphan disease therapy. *Orphanet. J. Rare Dis.*, **7**, 39.
2. Carter, C.O. (1977) Monogenic disorders. *J. Med. Genet.*, **14**, 316–320.
3. Baird, P.A., Anderson, T.W., Newcombe, H.B. and Lowry, R.B. (1988) Genetic disorders in children and young adults: a population study. *Am. J. Hum. Genet.*, **42**, 677–693.
4. Mazzucato, M., Visona Dalla Pozza, L., Manea, S., Minichiello, C. and Facchin, P. (2014) A population-based registry as a source of health indicators for rare diseases: the ten-year experience of the Veneto Region's rare diseases registry. *Orphanet J. Rare Dis.*, **9**, 37.
5. Boycott, K.M., Vanstone, M.R., Bulman, D.E. and MacKenzie, A.E. (2013) Rare-disease genetics in the era of next-generation sequencing: discovery to translation. *Nat. Rev.*, **14**, 681–691.
6. Scannell, J.W., Blanckley, A., Boldon, H. and Warrington, B. (2012) Diagnosing the decline in pharmaceutical R&D efficiency. *Nat. Rev. Drug Discov.*, **11**, 191–200.
7. Dharssi, S., Wong-Rieger, D., Harold, M. and Terry, S. (2017) Review of 11 national policies for rare diseases in the context of key patient needs. *Orphanet J. Rare Dis.*, **12**, 63.
8. Young, C.S. and Pyle, A.D. (2016) Exon skipping therapy. *Cell*, **167**, 1144.
9. Corey, D.R. (2017) Nusinersen, an antisense oligonucleotide drug for spinal muscular atrophy. *Nat. Neurosci.*, **20**, 497–499.
10. Nosengo, N. (2016) Can you teach old drugs new tricks? *Nature*, **534**, 314–316.
11. Corsello, S.M., Bittker, J.A., Liu, Z., Gould, J., McCarren, P., Hirschman, J.E., Johnston, S.E., Vrcic, A., Wong, B. and Khan, M. (2017) The drug repurposing hub: a next-generation drug library and information resource. *Nat. Med.*, **23**, 405–408.
12. Farooq, F., Abadía-Molina, F., MacKenzie, D., Hadwen, J., Shamim, F., O'Reilly, S., Holcik, M. and MacKenzie, A. (2013) Celecoxib increases SMN and survival in a severe spinal muscular atrophy mouse model via p38 pathway activation. *Hum. Mol. Genet.*, **22**, 3415.
13. Mears, A.J., Schock, S.C., Hadwen, J., Putos, S., Dyment, D., Boycott, K.M. and MacKenzie, A. (2017) Mining the transcriptome for rare disease therapies: a comparison of the efficiencies of two data mining approaches and a targeted cell-based drug screen. *NPJ Genomic Med.*, **2**, 14.
14. Chumakov, I., Milet, A., Cholet, N., Primas, G., Boucard, A., Pereira, Y., Graudens, E., Mandel, J., Laffaire, J., Foucquier, J. *et al.* (2014) Polytherapy with a combination of three repurposed drugs (PXT3003) down-regulates Pmp22 over-expression and improves myelination, axonal and functional parameters in models of CMT1A neuropathy. *Orphanet J. Rare Dis.*, **9**, 201.
15. van Paassen, B.W., van der Kooi, A.J., van Spaendonck-Zwarts, K.Y., Verhamme, C., Baas, F. and de Visser, M. (2014) PMP22 related neuropathies: Charcot–Marie–Tooth disease type 1A and hereditary neuropathy with liability to pressure palsies. *Orphanet J. Rare Dis.*, **9**, 38.
16. Churchill, G.A., Gatti, D.M., Munger, S.C. and Svenson, K.L. (2012) The Diversity Outbred mouse population. *Mamm. Genome*, **23**, 713–718.
17. Zuberi, A. and Lutz, C. (2016) Mouse models for drug discovery. Can new tools and technology improve translational power? *ILAR J.*, **57**, 178–185.
18. Petkov, P.M., Ding, Y., Cassell, M.A., Zhang, W., Wagner, G., Sargent, E.E., Asquith, S., Crew, V., Johnson, K.A., Robinson, P. *et al.* (2004) An efficient SNP system for mouse genome scanning and elucidating strain relationships. *Genome Res.*, **14**, 1806–1811.
19. Sun, W., Lee, S., Zhabotynsky, V., Zou, F., Wright, F.A., Crowley, J.J., Yun, Z., Buus, R.J., Miller, D.R., Wang, J. *et al.* (2012) Transcriptome atlases of mouse brain reveals differential expression across brain regions and genetic backgrounds. *G3 (Bethesda)*, **2**, 203–211.
20. Schock, S.C., Jolin-Dahel, K.S., Schock, P.C., Theiss, S., Arbuthnott, G.W., Garcia-Munoz, M. and Staines, W.A. (2012) Development of dissociated cryopreserved rat cortical neurons in vitro. *J. Neurosci. Methods*, **205**, 324–333.
21. Lesuisse, C. and Martin, L.J. (2002) Long-term culture of mouse cortical neurons as a model for neuronal development, aging, and death. *J. Neurobiol.*, **51**, 9–23.
22. von Bartheld, C.S., Bahney, J. and Herculano-Houzel, S. (2016) The search for true numbers of neurons and glial cells in the human brain: a review of 150 years of cell counting. *J. Comp. Neurol.*, **524**, 3865–3895.
23. Isaacson, J.S. and Scanziani, M. (2011) How inhibition shapes cortical activity. *Neuron*, **72**, 231–243.
24. Le Magueresse, C. and Monyer, H. (2013) GABAergic interneurons shape the functional maturation of the cortex. *Neuron*, **77**, 388–405.
25. Luhmann, H.J., Sinning, A., Yang, J.-W., Reyes-Puerta, V., Stuttgen, M.C., Kirischuk, S. and Kilb, W. (2016) Spontaneous neuronal activity in developing neocortical networks: from single cells to large-scale interactions. *Front. Neural Circuits*, **10**, 40.
26. Huang, D.W., Sherman, B.T. and Lempicki, R.A. (2009) Bioinformatics enrichment tools: paths toward the comprehensive functional analysis of large gene lists. *Nucleic Acids Res.*, **37**, 1–13.
27. Huang, D.W., Sherman, B.T. and Lempicki, R.A. (2009) Systematic and integrative analysis of large gene lists using DAVID bioinformatics resources. *Nat. Protoc.*, **4**, 44–57.

28. Krämer, A., Green, J., Pollard, J. and Tugendreich, S. (2014) Causal analysis approaches in ingenuity pathway analysis. *Bioinformatics*, **30**, 523–530.
29. Li, W.W., Le Goascogne, C., Schumacher, M., Pierre, M. and Courtin, F. (2001) Type 2 deiodinase in the peripheral nervous system: induction in the sciatic nerve after injury. *Neuroscience*, **107**, 507–518.
30. Courtin, F., Zrouri, H., Lamirand, A., Li, W.W., Mercier, G., Schumacher, M., Goascogne, C. and Le Pierre, M. (2005) Thyroid hormone deiodinases in the central and peripheral nervous system. *Thyroid*, **15**, 931–942.
31. Notterpek, L., Snipes, G.J. and Shooter, E.M. (1999) Temporal expression pattern of peripheral myelin protein 22 during in vivo and in vitro myelination. *Glia*, **25**, 358–369.
32. Gil-Ibanez, P., Garcia-Garcia, F., Dopazo, J., Bernal, J. and Morte, B. (2017) Global transcriptome analysis of primary cerebrocortical cells: identification of genes regulated by triiodothyronine in specific cell types. *Cereb. Cortex*, **27**, 706–717.
33. Gil-Ibanez, P., Bernal, J. and Morte, B. (2014) Thyroid hormone regulation of gene expression in primary cerebrocortical cells: role of thyroid hormone receptor subtypes and interactions with retinoic acid and glucocorticoids. *PLoS One*, **9**, e91692.
34. Dai, Y., Sangerman, J., Luo, H.Y., Fucharoen, S., Chui, D.H.K., Faller, D.V. and Perrine, S.P. (2016) Therapeutic fetal-globin inducers reduce transcriptional repression in hemoglobinopathy erythroid progenitors through distinct mechanisms. *Blood Cells. Mol. Dis.*, **56**, 62–69.
35. Hirst, R.C., McCullagh, K.J.A. and Davies, K.E. (2005) Utrophin upregulation in Duchenne muscular dystrophy. *Acta Myol.*, **24**, 209–216.
36. Hartley, M.D., Kirkemo, L.L., Banerji, T. and Scanlan, T.S. (2017) A thyroid hormone-based strategy for correcting the biochemical abnormality in X-linked adrenoleukodystrophy. *Endocrinology*, **158**, 1328–1338.
37. Finkel, R.S., Mercuri, E., Darras, B.T., Connolly, A.M., Kuntz, N.L., Kirschner, J., Chiriboga, C.A., Saito, K., Servais, L., Tizzano, E. *et al.* (2017) Nusinersen versus sham control in infantile-onset spinal muscular atrophy. *N. Engl. J. Med.*, **377**, 1723–1732.
38. Albinana, V., Bernabeu-Herrero, M.E., Zarrabeitia, R., Bernabeu, C. and Botella, L.M. (2010) Estrogen therapy for hereditary haemorrhagic telangiectasia (HHT): effects of raloxifene, on Endoglin and ALK1 expression in endothelial cells. *Thromb. Haemost.*, **103**, 441–534.
39. Wauters, E., Van Mossevelde, S., Van der Zee, J., Cruts, M. and Van Broeckhoven, C. (2017) Modifiers of GRN-associated frontotemporal lobar degeneration. *Trends Mol. Med.*, **23**, 962–979.
40. Liu, Z., Lv, Y., Zhao, N., Guan, G. and Wang, J. (2015) Protein kinase R-like ER kinase and its role in endoplasmic reticulum stress-decided cell fate. *Cell Death Dis.*, **6**, e1822.
41. Zinszner, H., Kuroda, M., Wang, X., Batchvarova, N., Lightfoot, R.T., Remotti, H., Stevens, J.L. and Ron, D. (1998) CHOP is implicated in programmed cell death in response to impaired function of the endoplasmic reticulum. *Genes Dev.*, **12**, 982–995.
42. Sano, R. and Reed, J.C. (2013) ER stress-induced cell death mechanisms. *Biochim. Biophys. Acta*, **1833**, 3460–3470.
43. Ferguson, L.B., Most, D., Blednov, Y.A. and Harris, R.A. (2014) PPAR agonists regulate brain gene expression: relationship to their effects on ethanol consumption. *Neuropharmacology*, **86**, 397–407.
44. Zhang, M., Luo, H., Xi, Z. and Rogaeva, E. (2015) Drug repositioning for diabetes based on 'omics' data mining. *PLoS One*, **10**, e0126082.
45. Li, J., Zhao, P., Yang, L., Li, Y., Tian, Y., Li, S. and Bai, Y. (2017) Integrating 3-omics data analyze rat lung tissue of COPD states and medical intervention by delineation of molecular and pathway alterations. *Biosci. Rep.*, **37**, 1–14.
46. Subramanian, A., Narayan, R., Corsello, S.M., Peck, D.D., Natoli, T.E., Lu, X., Gould, J., Davis, J.F., Tubelli, A.A., Asiedu, J.K. *et al.* (2017) A next generation connectivity map: L1000 platform and the first 1,000,000 profiles. *Cell*, **171**, 1437–1452.e17.
47. Lamb, J., Crawford, E.D., Peck, D., Modell, J.W., Blat, I.C., Wrobel, M.J., Lerner, J., Brunet, J.-P., Subramanian, A., Ross, K.N. *et al.* (2006) The connectivity map: using gene-expression signatures to connect small molecules, genes, and disease. *Science*, **313**, 1929–1935.
48. Nunez, B., Martinez de Mena, R., Obregon, M.J., Font-Llitjos, M., Nunes, V., Palacin, M., Dumitrescu, A.M., Morte, B. and Bernal, J. (2014) Cerebral cortex hyperthyroidism of newborn mct8-deficient mice transiently suppressed by lat2 inactivation. *PLoS One*, **9**, e96915.
49. Velasco, L.F.R., Togashi, M., Walfish, P.G., Pessanha, R.P., Moura, F.N., Barra, G.B., Nguyen, P., Rebong, R., Yuan, C., Simeoni, L.A. *et al.* (2007) Thyroid hormone response element organization dictates the composition of active receptor. *J. Biol. Chem.*, **282**, 12458–12466.
50. Kaneko, K., Sugeno, N., Tateyama, M., Misu, T., Suzuki, N. and Aoki, M. (2013) Hereditary neuropathy with liability to pressure palsy emerging after hypothyroidism. *Neurol. Clin. Neurosci.*, **1**, 160–161.
51. Adlkofer, K., Frei, R., Neuberg, D.H., Zielasek, J., Toyka, K.V. and Suter, U. (1997) Heterozygous peripheral myelin protein 22-deficient mice are affected by a progressive demyelinating tomaculous neuropathy. *J. Neurosci.*, **17**, 4662–4671.
52. Genin, E.C., Gondcaille, C., Trompier, D. and Savary, S. (2009) Induction of the adrenoleukodystrophy-related gene (ABCD2) by thyromimetics. *J. Steroid Biochem. Mol. Biol.*, **116**, 37–43.
53. Yuen, T., Iqbal, J., Zhu, L.-L., Sun, L., Lin, A., Zhao, H., Liu, J., Mistry, P.K. and Zaidi, M. (2012) Disease-drug pairs revealed by computational genomic connectivity mapping on GBA1 deficient, Gaucher disease mice. *Biochem. Biophys. Res. Commun.*, **422**, 573–577.
54. Qu, X.A. and Rajpal, D.K. (2012) Applications of connectivity map in drug discovery and development. *Drug Discov. Today*, **17**, 1289–1298.
55. Myerowitz, R., Lawson, D., Mizukami, H., Mi, Y., Tifft, C.J. and Proia, R.L. (2002) Molecular pathophysiology in Tay-Sachs and Sandhoff diseases as revealed by gene expression profiling. *Hum. Mol. Genet.*, **11**, 1343–1350.
56. Callizot, N., Combes, M., Steinschneider, R. and Poindron, P. (2011) A new long term in vitro model of myelination. *Exp. Cell Res.*, **317**, 2374–2383.
57. Jacobsen, K.X. and Staines, W.A. (2004) Vibration enhancement of slide-mounted immunofluorescence staining. *J. Neurosci. Methods*, **137**, 71–77.
58. Otto, F., Gortz, P., Fleischer, W. and Siebler, M. (2003) Cryopreserved rat cortical cells develop functional neuronal networks on microelectrode arrays. *J. Neurosci. Methods*, **128**, 173–181.
59. Illes, S., Theiss, S., Hartung, H.-P., Siebler, M. and Dihne, M. (2009) Niche-dependent development of functional

neuronal networks from embryonic stem cell-derived neural populations. *BMC Neurosci.*, **10**, 93.
60. Schulz, M., Iwersen-Bergmann, S., Andresen, H. and Schmoldt, A. (2012) Therapeutic and toxic blood concentrations of nearly 1, 000 drugs and other xenobiotics. *Crit. Care*, **16**, R136.
61. Robinson, M.D. and Oshlack, A. (2010) A scaling normalization method for differential expression analysis of RNA-seq data. *Genome Biol.*, **11**, R25.
62. Benjamini, Y. and Hochberg, Y. (1995) Controlling the false discovery rate: a practical and powerful approach to multiple testing. *J. R. Stat. Soc. Ser. B*, **57**, 289–300.